Mechanism of Microparticle Formation in the Compressed Antisolvent Precipitation and Photopolymerization (CAPP) Process

ARTICLE *in* LANGMUIR · APRIL 2003

Impact Factor: 4.46 · DOI: 10.1021/la0208272

3 AUTHORS, INCLUDING:

Kristi Anseth
University of Colorado Boulder
355 PUBLICATIONS **20,403** CITATIONS

Research Article

Mechanism of Microparticle Formation in the Compressed Antisolvent Precipitation and Photopolymerization (CAPP) Process

J. L. Owens, K. S. Anseth, and T. W. Randolph

Langmuir, **2003**, 19 (9), 3926-3934• DOI: 10.1021/la0208272 • Publication Date (Web): 02 April 2003

Mechanism of Microparticle Formation in the Compressed Antisolvent Precipitation and Photopolymerization (CAPP) Process

J. L. Owens,[†] K. S. Anseth,[†,‡] and T. W. Randolph*[,†,§]

Department of Chemical Engineering, Howard Hughes Medical Institute, and Center for Pharmaceutical Biotechnology, University of Colorado, Boulder, Colorado 80309-0424

Received October 3, 2002. In Final Form: February 28, 2003

We investigated the mechanism of particle formation in a new process that combines the principles of photopolymerization and compressed antisolvent processing. In this process, photopolymerization occurs when homogeneous solutions of monomer, initiator, and solvent are exposed to initiating light while being simultaneously introduced into a compressed antisolvent, which can result in highly cross-linked microparticles with a spherical morphology. The resulting particles, when examined using aerodynamic particle sizing, exhibit a bimodal particle size distribution. Ternary phase diagrams of antisolvent, monomer, and solvent solutions were measured and used to explain the mechanism(s) of particle formation. Specific concentration paths from the resulting ternary phase diagrams were investigated, and the significance of crossing the binodal, as well as the importance of where the binodal was crossed, was explained. In addition, manipulation of atomization conditions, varying process residence times, and nucleation rate calculations were used to further investigate the means of particle formation.

Introduction

We recently developed a new method that uses supercritical CO_2 to produce highly cross-linked polymeric microparticles.[1] In this technique, which we term compressed antisolvent precipitation and photopolymerization (CAPP), reactive multifunctional monomers and photoinitiators dissolved in a suitable diluent are injected into supercritical CO_2. After the monomer solution is injected into the CO_2, UV light is used to initiate photopolymerization in situ to produce cross-linked polymer microparticles. While such a process preserves the advantages of other supercritical CO_2 processes (environmentally benign, inexpensive antisolvent, low temperature processing, etc.), it also requires only minimal amounts of organic solvents and allows flexibility in their choice. For applications requiring biodegradable microparticles, the wide choice of available multifunctional monomer chemistries[2−4] provides a means for tailoring degradation and resultant additive release rates over a broad range of time scales.

Although we have successfully demonstrated that highly cross-linked microparticles can be formed in the CAPP process,[1] the detailed mechanism(s) that control their formation and determine the resulting particle size distributions are unknown. To provide better control of particle formation in the CAPP process, understanding of the mechanism(s) by which particles are formed is essential. In particular, we wish to explain the bimodal particle size distributions that we have observed under a variety of operating conditions and using various monomers.[1]

In the CAPP process, final particle size distributions potentially could be controlled by a number of mechanisms. First, the observed particle size distribution could be the result of photopolymerization of droplets of various sizes formed as a jet of monomer and solvent is atomized into CO_2. Bimodal particle size distributions have been observed during atomization in fuel injectors and ink jets.[5,6]

Second, particles could be formed from a reactive, homogeneous nucleation process. Free radical polymerization of monomer could occur in a homogeneous continuous phase. Nucleation of discrete particles could then be caused by decreased solubility as the polymer molecular weight increases. Bimodal particle size distributions could result from multiple growth rates (e.g., due to agglomeration of nascent particles and concomitant growth by polymerization). Kwauk and Debenedetti[7] observed bimodal particle size distributions in the rapid expansion in a supercritical solution (RESS) process and attributed them to a population of small particles resulting from very high nucleation rates and a population of larger particles resulting from postnucleation growth. Bimodal distributions have also been observed during spray drying from a variety of dilute solutions (100−500 ppm nonvolatile solute) and attributed to multiple nucleation and growth rates.[8,9]

Finally, the stream of monomer and solvent injected into CO_2 could undergo phase separation (e.g., a liquid−liquid phase split), followed by homogeneous nucleation and growth of particles by reactive addition in each of the resulting phases. Bimodal distributions would result from different rates of reaction (presumably due to different

* Corresponding author.
[†] Department of Chemical Engineering.
[‡] Howard Hughes Medical Institute.
[§] Center for Pharmaceutical Biotechnology.

(1) Owens, J. L.; Anseth, K. S.; Randolph, T. W. *Macromolecules* **2002**, *35*, 4289−4296.
(2) Metters, A. T.; Anseth, K. S.; Bowman, C. N. *Polymer* **2000**, *41*, 3993−4004.
(3) Muggli, D. S.; Burkoth, A. K.; Keyser, S. A.; Lee, H. R.; Anseth, K. S. *Macromolecules* **1998**, *31*, 4120−4125.
(4) Bruining, M. J.; Edelbroek-Hoogendoorn, P. S.; Blaauwgeers, H. G. T.; Mooy, C. M.; Hendrikse, F. H.; Koole, L. H. *J. Biomed. Mater. Res.* **1999**, *47*, 189−197.
(5) Bagley, S. T.; Gratz, L. D.; Johnson, J. H.; McDonald, J. F. *Environ. Sci. Technol.* **1998**, *32*, 1183−1191.
(6) Blazdell, P.; Kuroda, S. *Am. Ceram. Soc.* **2001**, *6*, 1257−59.
(7) Kwauk, X.; Debenedetti, P. G. *J. Aerosol Sci.* **1993**, *24*, 445−69.
(8) Lesniewski, T. K.; Friedlander, S. K. *Proc. R. Soc. London, Ser. A* **1998**, *454*, 2477−2504.
(9) Lesniewski, T. K.; Friedlander, S. K. *AIChE J.* **1997**, *43*, 2698−2703.

10.1021/la0208272 CCC: $25.00
Published on Web 04/02/2003

concentrations of reactants) found in each phase. Alternatively, a phase separation event could generate microdroplets of each phase, which would then photopolymerize to preserve the final particle size distribution.

We performed a series of experiments to elucidate the mechanism(s) of particle formation in the CAPP process. To test whether atomization of the reactant stream injected into supercritical CO_2 could explain the observed particle size distributions, we operated the CAPP process at a variety of injection nozzle Reynolds numbers and recorded the effect on particle size distributions. Nucleation and growth rates were estimated from CAPP-processed particle size distributions to provide further insight into the potential influence of atomization as a controlling mechanism.

To examine the effect(s) of phase behavior on particle formation in the CAPP process, ternary diagrams for poly(ethylene glycol) diacrylate monomers and methylene chloride, together with either a liquid antisolvent or supercritical CO_2, were constructed. Using the ternary diagrams, experiments involving various initial and final monomer/polymer concentrations were explored to discover the importance of the monomer concentration in the three-phase system composition on the resulting particles. Additionally, the particles were examined to determine if phase separation resulting from crossing the binodal suggests a particular particle formation pathway.

Materials and Methods

Materials. Photopolymerizable monomers used in these studies were poly(ethylene glycol) MW = 1000 diacrylate (PEG1000DA, Monomer-Polymer, Feasterville, PA) and poly(ethylene glycol) MW = 200 diacrylate (PEG200DA, Polysciences, Warrington, PA). PEG200DA was dried with molecular sieves (Aldrich, St. Louis, MO) during storage at 4 °C, and the solid PEG1000DA was purged with nitrogen gas (Airgas, Denver, CO) before storage at 4 °C. Methylene chloride (Fisher, Pittsburgh, PA) and methylnonafluoroisobutyl ether (HFE-7100, 3M, St. Paul, MN) were dried by storage over molecular sieves. The photoinitiator 2,2-dimethoxy-2-phenylacetophenone (DMPA, Ciba Geigy) was used as received. Carbon dioxide for the ternary phase diagram experiments (SFC Grade, Scott Specialty Gases, Plumsteadville, PA) and for the CAPP processing (Medical Grade, US Welding, Denver, CO) was used as received.

CAPP Processing of PEG200DA and PEG1000DA. We prepared cross-linked polymeric microparticles by injecting homogeneous multifunctional monomer, solvent, and photoinitiator solutions into a high-pressure chamber containing compressed CO_2 while simultaneously illuminating the chamber with high-intensity ultraviolet light. In particular, we studied diacrylated (DA) poly(ethylene glycol) (PEG) monomers that react to form highly cross-linked polymer networks.

The experimental apparatus for the CAPP process is described in detail elsewhere.[1] Medical grade CO_2 was deoxygenated and transferred to a syringe pump at a temperature of −10 °C. An additional pump contained the reactant solution. The high-pressure chamber was pressurized with deoxygenated CO_2 and allowed to equilibrate to 8.5 MPa at 35 °C. Reactant solutions for the photopolymerization CAPP process were prepared by dissolving monomer and photoinitiator in dry methylene chloride. The monomer−solvent−initiator solution was then pressurized to 8.5 MPa by a third pump. The solution was introduced into the chamber at a constant flow rate of 1 mL/min through a 100 μm quartz capillary nozzle. Concurrently, the CO_2 flowed at a constant rate of 25 mL/min through a heat exchanger (at 37 °C) followed by an 8.3 mm ($^1/_4$ in.) stainless steel tube into the high-pressure chamber. The quartz capillary tube was positioned in the center of the 8.3 mm ($^1/_4$ in.) tube while the CO_2 flowed in the annular region. Two high-intensity light sources (EFOS, Novacure, Mississauga, ON, Canada) with ultraviolet filters (320−500 nm band-pass) and fiber optic liquid light guides supplied the light to initiate the photopolymerization below the nozzle and through the borosilicate chamber windows. A 5 cm EFOS Light Line was used to spread the beam from one of the light guides to give a longer exposure path in the chamber as the particles passed by the illuminated windows. After injection and polymerization, the system was "washed" with several volumes of CO_2 before slow depressurization (∼30 min) at the operating temperature. After depressurization, the chamber was opened, and the particle product was collected for SEM analysis (see below) using a spatula from both the inside of the high-pressure chamber and a 0.2 μm filter at the outlet. Samples that were collected for Aerosizer analysis (see below) were collected only from the filter.

Particle Size Analysis. Particle size distributions were measured on a TSI Aerosizer (TSI 3325, St. Paul, MN) equipped with a dry powder particle disperser (TSI Aerodisperser 3230). Samples of roughly 0.05 g were dispersed in the Aerosizer and measured with the fine particle (0.1−200 μm) power setting. Particles were also attached to aluminum stubs using conductive tape and sputter-coated with a thin layer of gold before examination with a scanning electron microscope (SEM, ISI SX30).

Analysis of Double Bond Conversion within Particles. The double bond conversion in particles was measured by infrared spectroscopy. Using a mortar and pestle, particles were crushed and mixed with mineral oil to create a smooth paste of oil and crushed particles. The resulting paste was sandwiched between two KBr crystals, and a spectrum (64 scans averaged) was acquired in the mid-IR region (800−3000 cm^{-1}). The same technique was employed to make samples of the PEGDA monomers, and the double bond conversion was quantified by the ratio of the area of the carbon−carbon double bond doublet peak at 1635 cm^{-1} to the area of the internal carbonyl reference peak at 1725 cm^{-1} (which does not change appreciably during the polymerization) and compared to that same ratio for the unreacted monomer.

Particle Formation as a Function of Solvent Reynolds Number. Four replicate solutions of 25 wt % PEG1000DA in dry methylene chloride with 2% DMPA photoinitiator (relative to monomer) were prepared and CAPP-processed with solvent flow rates of 0.25, 0.5, 1, and 2 mL/min. The CO_2 flow rate was manipulated so that the total combined flow rate from the solvent and CO_2 lines was about 19 mL/min to give each system the same residence time and light dose in the high-pressure chamber. Particles were collected and analyzed using SEM and aerodynamic particle sizing, as described previously.

Nucleation and Growth Rate Calculations. Nucleation rates were calculated from population density curves created from particle size distribution data using a modified version of the method described by Randolph and Larson.[10] The assumptions in the analysis include the following: steady-state operation, ideal mixing, negligible agglomeration and fracture, size-independent growth of spherical particles, and unclassified withdrawal.

Under these assumptions, a semilog plot of the population density (number m^{-4}) versus particle size (m) gives a line whose intercept is n_0, the population density of nuclei, and slope is m, which is related to the growth rate, G (m s^{-1}), and process residence time, τ (s), by

$$m = \frac{-1}{2.303G\tau}$$

The particle nucleation rate, B (number m^{-3} s^{-1}), is defined as

$$B = n_0 G$$

CAPP Process Particle Formation as a Function of Light Dosage. The effect of changing the process residence time in the initiating UV light was examined to elucidate the effect of varying the dose of light on the resulting particle size distribution. To observe solely the effects of the change in residence time, the Reynolds number was held constant by manipulating both the size of the nozzle and the solution flow rate. Solutions of 25 wt % PEG1000DA in dry methylene chloride with 2 wt % (relative

(10) Randolph, A. W.; Larson, M. A. *Theory of Particulate Processes*, 2nd ed.; Academic Press: San Diego, CA, 1988.

Table 1. Experimental Conditions for the Testing of CAPP Processing Using Varied Process Residence Times

nozzle size (μm)	75	100	127
nozzle flow rate (mL/min)	0.75	1.0	1.27
nozzle Reynolds number	720	720	720
CO_2 flow rate (pump) (mL/min)	19	25	31
CO_2 flow rate (chamber) (mL/min)	31.2	41.6	52.0
avg particle residence time in light path (min)	3.2	2.4	1.9

to monomer) DMPA photoinitiator were processed using the CAPP method. All experiments were performed in triplicate. The residence time was manipulated while keeping the Reynolds number constant, by changing both the size of the nozzle and the CO_2 flow rate. Table 1 gives the exact conditions.

Construction of Liquid-Phase Ternary Diagrams. Young[11] and Mawson[12] used CO_2 as an antisolvent in its liquid form, as opposed to its supercritical state, to create particles in precipitation in a compressed antisolvent process. In addition, other CO_2-philic, liquid antisolvents have been successful replacements for high-pressure CO_2 in particle processing.[13] We chose one liquid antisolvent, HFE-7100 (methylnonafluoroisobutyl ether), to simulate CO_2 in the CAPP process with the PEG diacrylate monomer systems to help elucidate the mechanism(s) of particle formation for our system.

We examined two three-component systems, consisting of either the PEG1000DA or PEG200DA monomer, combined with dry methylene chloride (Fisher), and HFE-7100. Approximately 5−10 g of various methylene chloride/monomer mixtures of known compositions were prepared in 20 mL glass vials with small stir bars and heated in a mixing water bath at 35 °C and then cooled to −20 °C to minimize evaporation while adding portions of HFE-7100. Approximately 0.1 g of HFE-7100 was added, the vial was sealed, and the solution was placed in the 35 °C water bath for 30 min and then examined to determine whether one or two phases were present. If the solution was single phase, the sample was cooled again to −20 °C. Additional small amounts of HFE-7100 antisolvent were added until liquid−liquid phase separation at 35 °C was observed.

A liquid ternary phase diagram tie line was constructed by creating two identical solutions of 9 g of PEG1000DA, 9 g of HFE-7100, and 12 g of dry methylene chloride in 30 mL sealed separatory funnels, and the solutions were heated to 35 °C. The solutions phase separated, and each phase was drawn off, sealed to prevent evaporation, and weighed. After weighing, the HFE-7100 and the methylene chloride were allowed to evaporate, and the remaining PEG1000DA was quantified. The combination of the initial composition and the concentration calculated from the previously described experiment gives the approximate tie line.

PEGDA Particle Formation in HFE-7100. *PEG1000DA.* Using the ternary diagrams created as described in the previous section, several experiments were designed to elucidate the importance, if any, of crossing the binodal. On a ternary diagram, the binodal separates the single-phase region from the two-phase region, and the point at which the binodal is crossed determines the mechanism by which phase separation occurs.[14]

Two solutions of 25% PEG1000DA (with 2 wt % (relative to monomer) DMPA photoinitiator) in methylene chloride were introduced (as described in detail below) into a mixture of HFE-7100 and methylene chloride. In the first case, the binodal was not crossed, while, in the second case, the binodal was crossed, somewhat close to the plait point.

PEG200DA. Five solutions of PEG200DA (with 2 wt % (relative to monomer) DMPA photoinitiator) in methylene chloride (10, 25, 40, 55, and 70 wt % PEG200DA, respectively) were prepared. These solutions were injected into a mixture of HFE-7100 and methylene chloride, as described in detail below.

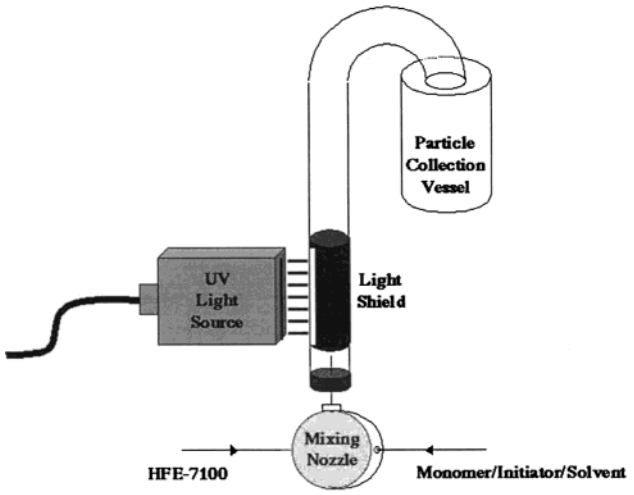

Figure 1. Schematic for CAPP processing of PEGDAs with the HFE-7100 system.

Apparatus for Production of Particles Using Liquid Mimics of CO_2. The apparatus used to mimic the CAPP process and produce particles from the concentration paths in the HFE-7100 liquid antisolvent is outlined in Figure 1. A 1.2 cm i.d. glass tube with a length of 36 cm was heated and bent as shown in the figure. On the bottom of the tube, a rubber septum (Fisher, Pittsburgh, PA) was fitted tightly and a 100 μm quartz capillary tube was inserted through the septum into the glass tube. The capillary was the outlet from a mixing nozzle (Microtee, Valco) with a mixing volume of 0.1 μL through which two solutions, the mixture of HFE-7100 and methylene chloride and that of methylene chloride and the PEGDA monomers, flowed. The total solution flow rate was held constant at 1.13 mL/min, and the ratios of the various components were manipulated to obtain particular points from the ternary diagrams. About 5 mm above the outlet of the capillary, a 5 cm EFOS Light Line connected to an EFOS Novacure operating at 5500 mW/cm^2 (measured with the Novacure Radiometer) with a 320−500 nm band-pass filter was used to initiate the polymerization. A dark paper shield was used to contain the light within the 5 cm section of the glass tube. The solution in which particles were suspended was collected at the mouth of the glass tube. Because drying of the liquid suspensions to produce samples that could be analyzed using the Aerosizer could have resulted in artifacts, the particle suspensions were analyzed by light scattering using a Malvern Mastersizer to determine the particle size distributions.

Construction of High-Pressure Ternary Diagrams. High-pressure ternary phase diagrams of systems containing methylene chloride, carbon dioxide, and PEGDA were created to help determine the mechanism of formation of the particles in the CAPP process. The high-pressure cell used for these experiments was constructed of stainless steel. On each end, sapphire windows 5 mm in diameter were contained between Teflon spacers and were fixed into place with large bolts. There were three ports on the sides of the cell for the CO_2 inlet, pressure transducer outlet, and sample introduction. The heating element contacted the cell over the entire bottom half of the cell, as well as two of the three inlet/outlet port bolts. Cell volume was measured by quantifying the volume of liquid CO_2 at 20 MPa and 25 °C that was pumped into the cell. The cell volume (including the valves and attached tubing) was determined to be 3.90 ± 0.02 mL. The temperature in the cell was measured with temperature transducers (CN76000, Omega) and ceramic thermocouples located directly above and below the cell. The pressure in the cell was measured using a pressure transducer (710 Digiquartz, Paroscientific Inc.).

The high-pressure cell was initially charged with a known quantity of a mixture of methylene chloride and PEGDA. The system was then closed, the temperature controller was activated, and the system was heated to 35 °C. During heating, the CO_2 syringe pump was held at a constant pressure of 8.5 MPa. After a constant system temperature of 35 °C was reached, the CO_2 valve was opened for a short period of time to introduce CO_2 into the cell and then quickly closed to prevent the other components

(11) Young, T. J.; Johnston, K. P.; Mishima, K.; Tanaka, H. *J. Pharm. Sci.* **1999**, *88*, 640−650.
(12) Mawson, S.; Kanakia, S.; Johnston, K. P. *J. Appl. Polym. Sci.* **1997**, *64*, 2105−2118.
(13) Sarkari, M.; Darrat, I.; Knutson, B. L. *AIChE J.* **2000**, *46*, 1850−1859.
(14) Dixon, D. J.; Johnston, K. P. *J. Appl. Polym. Sci.* **1993**, *50*, 1929−1942.

from escaping out the CO_2 inlet line. The system was allowed to equilibrate, which generally reduced the system pressure as components mixed, until the pressure stabilized, at which time more CO_2 was added. This process was repeated until the pressure stabilized at 8.49 ± 0.02 MPa.

Next, the contents of the cell were inspected to determine if the mixture was one- or two-phase. Using a flashlight, two dental mirrors, and a magnifying glass, the contents of the cell were relatively easy to observe visually. Because the presence of a second phase was not always obvious, stirring was turned on and off to observe the two phases, which often appeared to have only a very slight difference in refractive indices.

Finally, the amount of CO_2 introduced into the cell was measured with a 2 L graduated cylinder. The cylinder was originally filled with water, and the initial volume was measured. The water was previously saturated with carbon dioxide for 10 min. Additionally, the water reservoir contained excess activated charcoal to remove the organic solvent following the introduction of the cell contents. After all the valves of the cell were closed, the outlet valve was opened, the contents of the cell were quickly released into the cylinder, and the final volume of the cylinder was recorded. The pressure and temperature of the ambient atmosphere were measured using a pressure transducer (Digiquartz 710, Paroscientific, Inc.) and a mercury thermometer, respectively.

For points on the diagram that required ~25% CO_2 and less, an additional syringe pump (ISCO) was necessary to introduce the methylene chloride into the cell. For these experiments, the cell was initially charged with PEGDA of a known amount using a micropipet (Oxford Benchmate, Nychiryo) and all valves were closed, save for the valve which connected to the pressure transducer. Next, methylene chloride in the pump charged to ~8.3 MPa was allowed into the cell by opening (and promptly closing) the solvent feed valve. The initial amount of methylene chloride in the syringe pump was recorded prior to opening the solvent feed valve and recorded after the valve was closed, so the total volume of methylene chloride introduced into the cell was known. Finally, the valve to the CO_2 pump, operating in constant pressure mode at 8.5 MPa, was opened (and promptly closed) and the cell equilibrated to 8.49 ± 0.02 MPa. The volume of CO_2 was measured as described previously.

The volume of the CO_2 measured at ambient temperature and pressure was converted to a mass of CO_2 using a modified Peng−Robinson equation of state.[15] Since known masses of the methylene chloride and PEG200DA were introduced into the chamber, the total mass of the three components in the cell could be calculated as well as the weight percentages of each of the three components.

CAPP Process Particle Formation as a Function of Solvent to Antisolvent Ratio. The effect of changing the ratio of solvent/monomer solution to the CO_2 antisolvent was explored in a series of experiments. Solutions of 25 wt % PEG1000DA in dry methylene chloride with 2 wt % (relative to monomer) DMPA photoinitiator were processed using the CAPP method at 8.5 MPa and 35 °C, and all experiments were performed in triplicate. The solvent/monomer to antisolvent ratio was manipulated by changing both the size of the nozzle and the solvent/monomer flow rate. The Reynolds number through the nozzle and residence time in the chamber were held constant to specifically examine the effects of changing the ratio of the solvent/monomer solution to the CO_2 antisolvent on the resulting particle size distribution. The volume ratios of methylene chloride solution and CO_2 were calculated using a modified Peng−Robinson equation of state[16] and a Peng−Robinson equation of state with an extended corresponding states model,[15] respectively. Table 2 summarizes the precise experimental conditions.

CAPP Process Particle Formation as a Function of Monomer Concentration. Four solutions of 25, 35, 40, and 45 wt % PEG200DA in dry methylene chloride with 2% DMPA photoinitiator (relative to monomer) were fashioned and CAPP-processed with a solvent flow rate of 1 mL/min and a CO_2 flow rate of 19 mL/min, so that the residence time and dose of light in the high-pressure chamber was the same for each monomer concentration. All experiments were performed in duplicate. The resulting particles were collected and analyzed using SEM and aerodynamic particle sizing, as described previously.

Table 2. Experimental Conditions for the Testing of CAPP Processing Using Varied Antisolvent to Monomer/Solvent Ratios

nozzle size (μm)	75	100	127
nozzle flow rate (mL/min)	0.75	1.0	1.27
nozzle Reynolds number	720	720	720
CO_2 flow rate (pump) (mL/min)	25	25	25
CO_2 flow rate (chamber) (mL/min)	41.6	41.6	41.6
avg particle residence time in light path (min)	2.4	2.4	2.4
fraction CO_2	96.4	95.2	94
fraction methylene chloride	2.7	3.6	4.5
fraction PEG1000DA	0.9	1.2	1.5

Results and Discussion

CAPP Process Particle Formation as a Function of Solvent Flow Reynolds Number. Solvent flow rate (and consequently the Reynolds number) was changed over 2 orders of magnitude during CAPP processing of PEG1000DA. Flows in a typical jet exhibit a transition between laminar and turbulent flow at a critical Reynolds number, Re_{crit}, according to[17]

$$Re_{crit} = 12000\left(\frac{1}{d}\right)^{-0.3} \quad (1)$$

where d is the diameter of the solvent flow capillary nozzle, which was 100 μm in this case. For these experiments, $Re_{crit} = 760$, so the particular Reynolds numbers applied in this experiment were varied over the range of laminar, transitional, and turbulent flows. All of the resulting size distributions were bimodal (data not shown), with one population at about 2 μm and a second population at about 30 μm. Only minor differences between the size distributions were seen as a function of Reynolds number (data not shown). Apparently, wide changes in the characteristics of the solvent flow have little effect on the resulting particle size distribution, suggesting that jet atomization is not a controlling factor.

Nucleation and Growth Rate. Figure 2 shows the resulting population density curves calculated from a representative particle size distribution of CAPP-processed PEG1000DA. The resulting multimodal curve gives two nucleation and growth rates when linear regressions were fit to each mode of the data. In traditional nucleation and growth processes, biphasic population density distributions and nonlinear population density plots can result from impurities,[18] nonuniform concentration gradients within the reaction volume,[10] particles resulting from both primary and secondary nucleation,[10] agglomeration of primary particles,[19] or failure of the previously listed model assumptions.

These calculations for CAPP-processed PEG1000DA particles allow us to calculate two apparent nucleation rates of 9×10^9 and 1×10^8 number m^{-3} s^{-1}. Both of these rates are significantly higher than nucleation rates typically observed in liquids.[20] Additionally, the nucleation rates fall between those reported for precipitation of

(15) Span, R.; Wagner, W. *J. Phys. Chem. Ref. Data* **1996**, *25*, 1509−1596.

(16) *NIST Thermophysical Properties of Hydrocarbon Mixtures*, 2nd ed.; NIST: Gaithersburg, MD, 2001.

(17) Van de Sante, G.; Smith, J. M. *Chem. Eng. Sci.* **1976**, *31*, 219−224.

(18) White, E. T.; Bendig, L. L.; Larson, M. A. *AICHE Symp. Ser.* **1976**, *72*, 41−47.

(19) Hoyt, R. C. *Precipitation kinetics of a continuous precipitator with application to precipitation of ammonium polyurinate*; University of Iowa: Ames, IA, 1978.

(20) Liang, B.; Hartel, R. W. *J. Cryst. Growth* **1991**, *108*, 129−142.

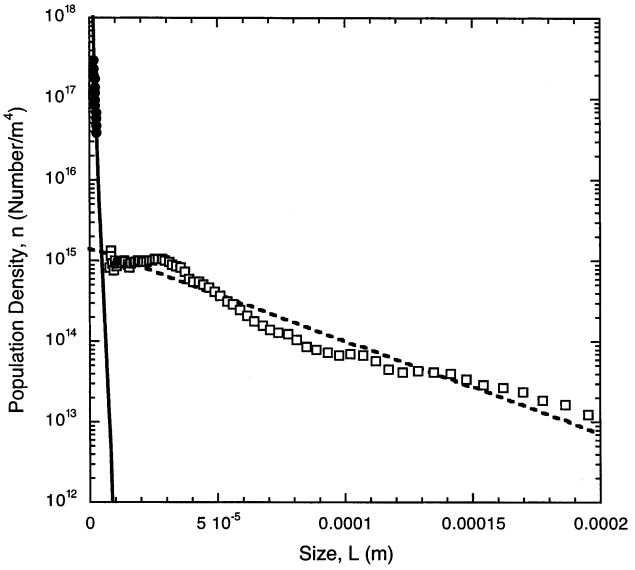

Figure 2. Semilog population density plot from CAPP-processed PEG1000 microparticles.

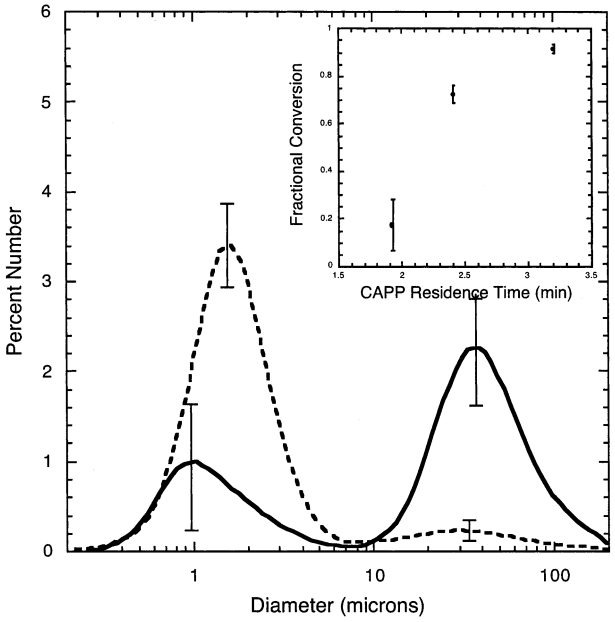

Figure 3. Particle size distributions of CAPP-processed PEG1000DA particles created with different residence times of 2.4 min (- - -) and 3.2 min (—). The data are shown as smoothed curves of the mean of triplicate experiments, and the error bars represent one standard deviation of the mean for the selected sizes shown. The inset graph shows fractional conversion of double bonds in particle samples as a function of process residence time.

solutes following rapid expansion of homogeneous supercritical solutions (10^{23} number m^{-3} s^{-1})[21−23] and gas antisolvent (GAS) (10^{8} number m^{-3} s^{-1})[24] processes, which suggests that the nucleation and growth fall in the realm of supercritical fluid processes. However, the calculated growth rates of 1.5×10^{-9} and 1.1×10^{-7} m/s are similar to crystallization growth kinetics in liquids[25−27] and are around 6 orders of magnitude lower than those in other supercritical processes.[28] The slower growth rate is likely the result of liquid-phase growth processes, either liquid−liquid phase separation or growth due to polymerization. The nonlinearity of the second mode of the population density plot, illustrated by the hollow square data points in Figure 2, suggests size-dependent growth. Although size-dependent growth is not typically seen in other supercritical fluid processes, it can be characteristic of reaction driven growth as well as growth of solid particles in liquids.[10] Therefore, we cannot exclude nucleation and growth as a method of particle formation for the CAPP process.

CAPP Process Particle Formation as a Function of Light Dose. Figure 3 illustrates the drastic change in the particle size distributions with a relatively small change in the residence time in the UV light. The process conditions are outlined in Table 1. The process residence times varied from 1.9 to 3.2 min. Increasing the residence time of the process results in larger particles. For the shorter residence time of 2.4 min, a greater proportion of the particles are in the smaller mode between about 0.5 and 10 μm. When the process residence time is increased, most of the particles are larger, in the range 10−200 μm. This shift to larger particles suggests that the particle growth process is strongly influenced by the photopolymerization, since the particles that spent a longer time in the light were significantly larger than those produced with a shorter time in the light. This is likely due to agglomeration of the smallest particles to form larger particles, because as light dose increases, the population of smaller particles is depleted and that of the larger particles increases, but their respective median sizes do not change appreciably.

Also shown in Figure 3 is a graph displaying fractional conversion of double bonds of particle samples collected from the filter as a function of residence time. Although the experiments with the 1.9 min residence time did not result in discrete particles, we were able to collect partially polymerized agglomerates from the filter. As the residence time of the polymerizing particles in the CAPP process is increased, the fractional conversion of the resulting particles also increases. This result is significant, as it allows the creation of particles with specific levels of conversion, which can be easily manipulated with the process conditions. The ability to tailor the conversion could make this process useful for a variety of applications.

Construction of Liquid-Phase Ternary Diagrams and CAPP Processing of PEGDAs in HFE-7100. Liquid antisolvents have been useful in PCA-style particle processing techniques.[11−13] We utilized the liquid antisolvent HFE-7100 (methylnonafluoroisobutyl ether) in the CAPP process with the PEG diacrylate monomer systems to help elucidate the mechanism(s) of particle formation for our system. We endeavored to explain the CAPP process particle formation by examining the ternary phase behavior of the CAPP process components and varying the kinetics of phase separation during the CAPP process by crossing the binodal boundary at various points along the two-phase boundary.

Figure 4a shows the resulting ternary phase diagram for the PEG1000DA/methylene chloride/HFE-7100 system (solid points). The single-phase region is located between the solvent/monomer axis and the binodal (denoted by the points in Figure 4a). The two-phase region, which

(21) Debenedetti, P. G.; Tom, J. W.; Kwauk, X.; Yeo, S. D. *Fluid Phase Equilib.* **1993**, *82*, 311−321.
(22) Debenedetti, P. G. *AIChE J.* **1990**, *36*, 1289−98.
(23) Turk, M. *J. Supercrit. Fluids* **2000**, *18*, 169−184.
(24) Chang, C. J.; Randolph, C. J. *AIChE J.* **1990**, *36*, 939−942.
(25) Gomez-Morales, J.; Torrent-Burgues, J.; Rodriguez-Clemente, R. *Cryst. Res. Technol.* **2001**, *36*, 1065−1074.
(26) Tanrikulu, S. U.; Eroglu, I.; Bulutcu, A. N.; Ozkar, S. *J. Crystal Growth* **2000**, *208*, 533−540.
(27) Wojcik, J. A.; Jones, A. G. *Chem. Eng. Res. Des.* **1997**, *75*, 113−118.
(28) Bristow, S.; Shekunov, T.; Shekunov, B. Y.; York, P. *J. Supercrit. Fluids* **2001**, *21*, 257−271.

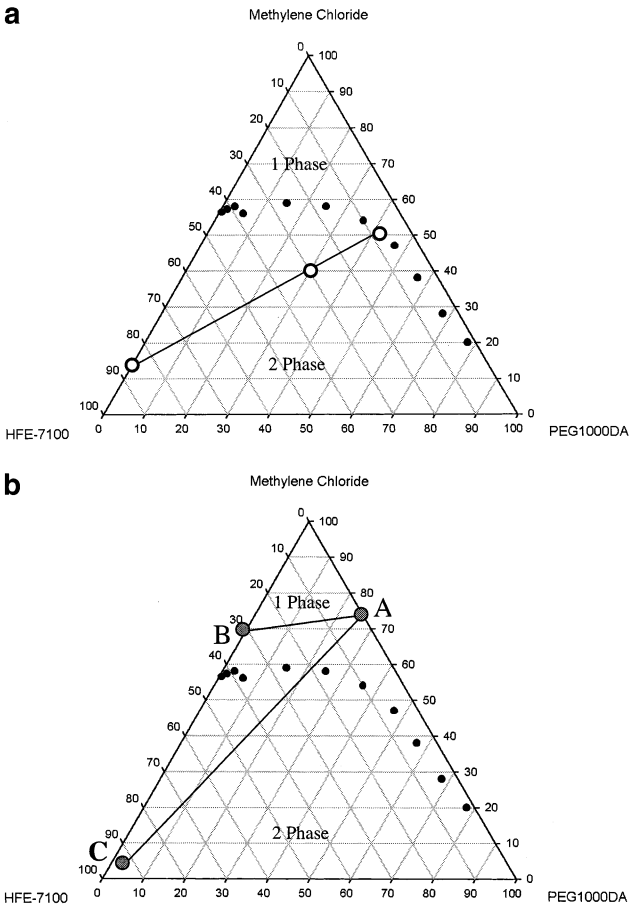

Figure 4. (a) Resulting tie-line from the phase separation of a 30 wt % PEG1000DA, 30 wt % HFE-7100, and 40 wt % methylene chloride solution. (b) Concentration paths on the PEG1000DA ternary diagram. Point A represents a 25% solution of PEG1000DA in methylene chloride. Points B and C represent the final compositions when the solution represented by point A is introduced into a solution of (B) 30% HFE and 70% methylene chloride and (C) 97% HFE and 3% methylene chloride.

includes both metastable and unstable regions separated by the spinodal, is positioned between the binodal and the HFE-7100/monomer axis. The polymer-lean section of the binodal appears to be located at a monomer concentration that approaches zero.

Figure 4a also shows results from a single tie line experiment performed in duplicate. A solution nominally composed of 30 wt % PEG1000DA, 30 wt % HFE-7100, and 40 wt % methylene chloride will phase separate into two phases, one containing roughly 41 wt % monomer and one with no measurable PEG1000DA. This experiment was used to demonstrate the approximate slope of the ternary diagram tie lines, so that reasonable assumptions regarding the phase separation process could be made. Results from these experiments rule out the possibility of tie lines parallel to the solvent/antisolvent axis, which would result in two phases, each with the same monomer concentration. In addition, the approximate tie lines further aid in the explanation of particle formation mechanisms, since the resulting tie line allows us to approximate the compositions of polymer-rich and polymer-lean phases.

When a solution with an overall concentration represented by point A in Figure 4b is CAPP-processed under the conditions previously described, following the path to point B instead of point C, no particles result. Therefore,

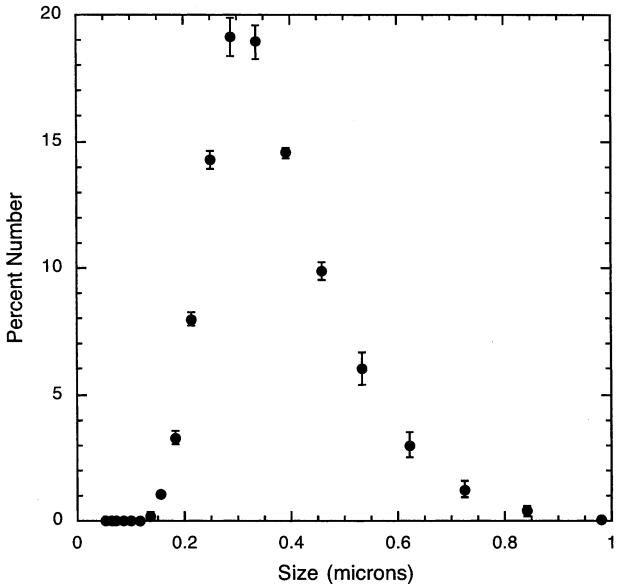

Figure 5. Particle size distribution from CAPP processing on path A (25% solution of PEG1000DA in methylene chloride with DMPA photoinitiator) to point C (97% HFE-7100 and 3% methylene chloride) illustrated in Figure 4b. The data shown are the mean of triplicate experiments, and the error bars represent one standard deviation of the mean for the selected sizes shown.

to form particles, the solubility line must be crossed and phase separation must occur. Additionally, this result shows that polymerization does not generate particles in the continuous phase, at least at the low concentration of monomer represented by point B, which rules out this explanation for our bimodal particle size distribution.

Particles were formed when the concentration path from point A to point C was followed. This trajectory crosses the binodal on the ternary phase diagram, causing phase separation to occur. The resulting particle size distribution is shown in Figure 5. The distribution is unimodal, with an average particle size of $0.28 \pm 0.09\,\mu$m based on analysis of particles collected in triplicate experiments. This unimodal distribution might be expected, since this path crosses approximately through the plait point, where phase separation results in equal concentrations of monomer in both the monomer-rich and monomer-lean phases. Alternatively, as the monomer-lean axis is very near the 0% monomer axis, one would not expect a bimodal particle size distribution resulting from phase separation and polymerization within each phase.

Unfortunately, since the location of the spinodal is unknown (and is nontrivial to calculate), we do not know if the final point C (Figure 4b) is in the unstable or metastable region of the graph and, therefore, cannot specifically identify if phase separation occurs by nucleation and growth, as would be the case if the spinodal was not crossed, or by spinodal decomposition, as would be the case if the spinodal was crossed. It is likely that, by processing on the path from A to C, the solution undergoes spinodal decomposition, causing separation into polymer-rich and polymer-lean phases, depending on how quickly point C is approached and whether point C is in the metastable region. Processing on the path from point A to point C, the path crosses on or very near the plait point, where the binodal and spinodal coincide. Crossing at the plait point ensures phase separation by spinodal decomposition as opposed to nucleation and growth. The path from A to C allows either possible mechanism of phase separation, depending upon the location of the spinodal.

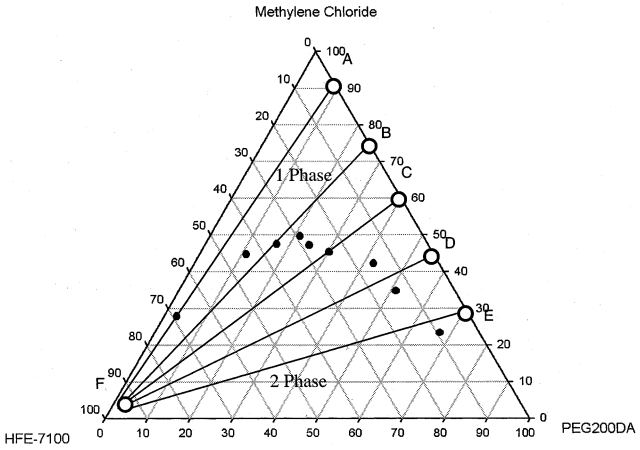

Figure 6. Concentration paths of the PEG200DA/methylene chloride/HFE-7100 ternary diagram. Solutions containing various molar ratios of PEG200DA/methylene chloride (points A−E) were injected into HFE-7100 to form mixtures with overall mole fractions represented by point F.

The ternary phase diagram for the PEG200DA/methylene chloride/HFE-7100 system is demonstrated in Figure 6. This phase diagram contains several important differences from the similar PEG1000DA system. First, the binodal of the PEG200DA system required less methylene chloride solvent than that of the PEG1000DA system, which is to be expected due to greater solubility of the smaller PEG200DA molecule in the methylene chloride/HFE-7100 mixture. Also, the polymer-lean section of the binodal does not coincide with the 0% monomer axis, which allows exploration into the phase behavior and particle production when a significant portion of the monomer is located in the continuous phase.

Similar experiments to those discussed in the previous section were performed with the PEG200DA monomer to discover the effect of crossing the binodal at different concentrations. This is especially important with the PEG200DA system, where the monomer-lean section of the binodal is not approximated at the 0 wt % monomer axis as with the PEG1000DA system. Figure 6 illustrates the concentration paths explored in the ternary system of PEG200DA/methylene chloride/HFE-7100. Three solutions at each of the points A−E were injected into a solution of approximately 3 wt % methylene chloride and 97% HFE-7100, such that the final nominal compositions were represented by point F. Figure 7 shows the average particle size distributions for each of the runs from the PEG200DA ternary diagram.

Solutions of composition represented by point A (Figure 6) were injected into HFE-7100, resulting in a final nominal composition represented by point F. Formation of particles did not result, as the path likely did not cross into the two-phase region. Injecting on paths from points C, D, and E to point F resulted in particles with bimodal particle size distributions. When crossing approximately through the plait point on the path between points B and F, the resulting particles again have a unimodal distribution. This suggests that phase separation upon the crossing of the binodal dominates the resulting particle size distribution. The separation into two phases, one monomer rich and the other monomer lean, would result in two different sizes of particles, since each phase containing vastly different amounts of monomer should exhibit different polymerization and growth rates due to the difference in monomer concentrations.

High-Pressure Ternary Diagrams. Figure 8a shows the ternary phase diagram of PEG1000DA, methylene chloride, and CO_2 experimentally determined at 8.5 MPa and 35 °C, where the open diamonds represent concentrations in the two-phase region and the black circles represent one-phase mixtures. The binodal is located between the single-phase and two-phase regions represented by the black circles and open diamonds, respectively. This representation of the ternary phase diagram is different from those constructed with the liquid antisolvent, which show the approximate binodal. In this case, the transition between one and two phases was not easily observed while keeping the system pressure constant at approximately 8.5 MPa, so points on either side of the binodal, corresponding to one- and two-phase solutions, were measured. Only about half of the diagram was constructed because of the time necessary to reach equilibrium at high monomer concentrations; the two points (open diamonds) at roughly 30 wt % monomer in Figure 8a each took upward of 50 h to reach equilibrium, likely due to mixing limitations of the apparatus and the lengthy time necessary for CO_2 to diffuse into the polymer/solvent mixture. Additionally, the system plumbing made it impossible to introduce very small amounts of CO_2 necessary to obtain points on the monomer-rich section of the diagram. The portion of the diagram that was constructed includes the region of interest consistent with the operating concentrations in the CAPP process. The data point (black circle) corresponding to 75 wt % methylene chloride and 25 wt % CO_2 confirms that CO_2 and methylene chloride are miscible at supercritical conditions, which is consistent with their binary phase behavior.[29] Compared to the ternary diagram formed using the liquid antisolvent HFE-7100, less methylene chloride is required to create single-phase mixtures. Additionally, the approximate plait point is shifted toward the monomer-lean side of the diagram, as also seen in the liquid ternary system. The chief difference between the liquid and high-pressure diagrams is that the binodal for the CO_2 system does not coincide with the 0% monomer axis.

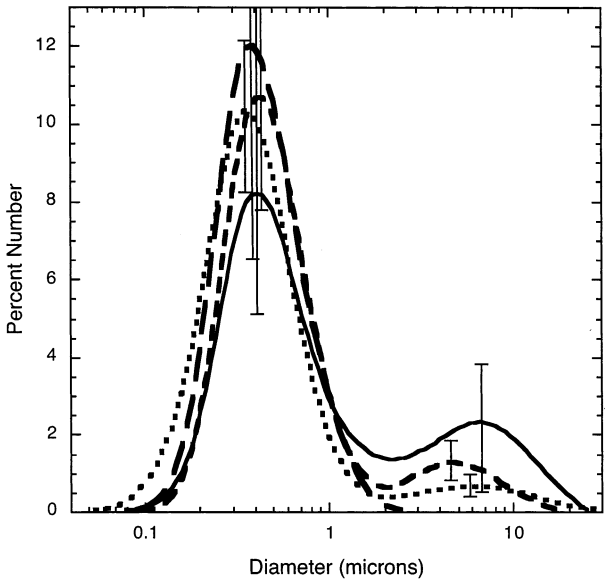

Figure 7. Particle size distributions from CAPP-processing paths on the HFE-7100/PEG200DA/methylene chloride ternary diagram (Figure 6). Particle size distributions are for path B to F (— — —), path C to F (· · ·), path D to F (- - -), and path E to F (—). The data are shown as smoothed curves of the mean of triplicate experiments, and the error bars represent one standard deviation of the mean for the selected sizes shown.

(29) Gonzalez, A. V.; Tufeu, R.; Subra, P. *J. Chem. Eng. Data* **2002**, *47*, 492−495.

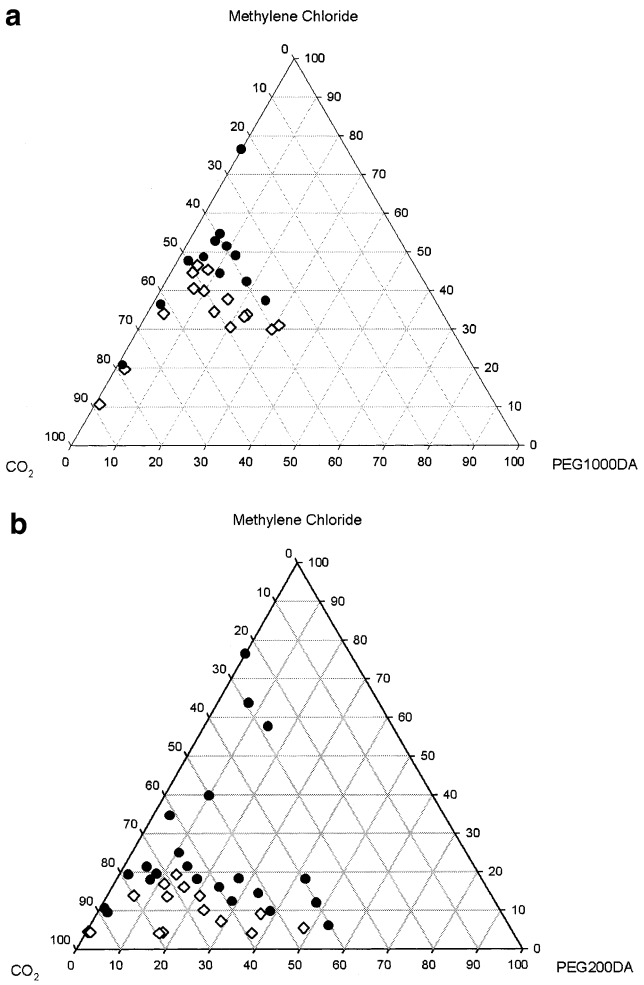

Figure 8. (a) Ternary diagram of PEG1000DA, methylene chloride, and CO_2 at 85 bar and 35 °C. The black circles (●) represent solutions in the one-phase region and open diamonds (◇) represent solutions in the two-phase region. (b) Ternary diagram of PEG200DA, methylene chloride, and CO_2 at 85 bar and 35 °C. The black circles (●) represent solutions in the one-phase region, and open diamonds (◇) represent solutions in the two-phase region.

Figure 8b is the ternary phase diagram of PEG200DA, methylene chloride, and CO_2 experimentally determined as described previously at 8.5 MPa and 35 °C. The open diamonds represent concentrations in the two-phase region, the black circles represent one-phase mixtures, and the binodal is located between these two regions. Again, compared to the ternary diagram formed using the liquid antisolvent HFE-7100, significantly less methylene chloride is required to create single-phase mixtures. Additionally, compared to the liquid ternary diagram, the approximate plait point is shifted toward the monomer-lean side of the diagram.

CAPP Process Particle Formation as a Function of Monomer/Solvent to Antisolvent Ratio. The resulting particle size distributions from experiments outlined in Table 2 are shown in Figure 9. These experiments explored the effect of changing the ratios of CO_2, monomer, and solvent on the resulting particle size distributions. The residence time was held constant at 2.4 min, and the estimated mass fractions of CO_2, monomer, and methylene chloride are shown in Table 2 for each of the three cases. The resulting particle size distributions are bimodal with both modes of the data covering the similar particle size regions. No apparent effect on the resulting particle size distributions is

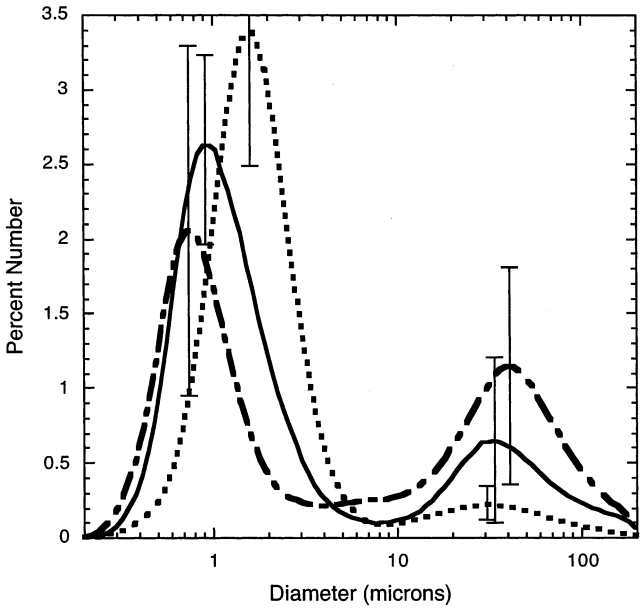

Figure 9. Particle size distribution of CAPP-processed particles created using various ratios of solvent solution to CO_2 for 1.5 wt % PEG1000DA (– – –), 0.9 wt % PEG1000DA (—), and 1.2 wt % PEG1000DA (- - -). The data are shown as smoothed curves of the mean of triplicate experiments, and the error bars represent one standard deviation of the mean for the selected sizes shown.

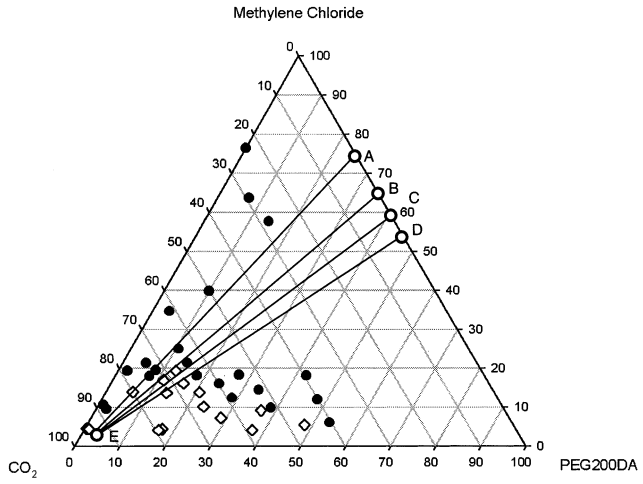

Figure 10. Concentration paths from the PEG200DA/methylene chloride/CO_2 ternary diagram. The black circles (●) represent solutions in the one-phase region, and open diamonds (◇) represent solutions in the two-phase region.

observed with small changes in the ratio of each of the three components. This result suggests that small changes in the final composition do not greatly influence the resulting particle size distribution. This could be due to a rapid phase separation as the mixture crosses the binodal, which would prevent the nominal composition from being reached before particle formation has occurred.

CAPP Process Particle Formation as a Function of Initial Monomer Concentration. Figure 10 illustrates the experimental paths explored in the ternary system PEG200DA/methylene chloride/CO_2, and Figure 11 shows the resulting particle size distributions. As the monomer concentration was changed between 25 and 35 wt % (point A to point B in Figure 10), a dramatic change in the resultant particle size distribution was observed. The distribution for the 25% monomer solution has distinct peaks between 0.2 and 10 μm and 10 and 200 μm, while,

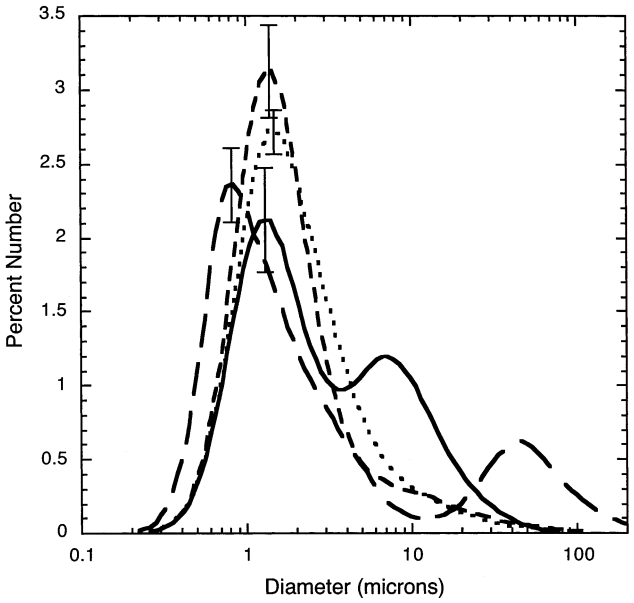

Figure 11. Particle size distributions from CAPP processing on the HFE-7100/PEG200DA/methylene chloride ternary diagram (Figure 10). Path A to E (– – –), path B to E (—), path C to E (- - -), and path D to E (• • •). The data are shown as smoothed curves of the mean of triplicate experiments, and the error bars represent one standard deviation of the mean for the selected sizes shown.

in the 35% solution, the two peaks combine between 0.2 and 50 μm. As the concentration is further increased to 40 and 45% PEG200DA monomer (points C and D in Figure 10) and the path is closer to the approximate plait point denoted in Figure 10, the resulting particle size distribution becomes unimodal, with small numbers of particles observed over 10 μm.

These results suggest that the composition at which the binodal is crossed dominates the modality of the particle size distributions. Furthermore, this set of experiments demonstrates the ability to manipulate the particle size distributions created in the CAPP process on the basis of initial monomer concentrations, a variable that is easily controlled.

Conclusions

Analysis of the ternary phase diagram for CO_2, methylene chloride, and acrylated monomer suggests that the mechanism for particle formation in the CAPP process is dominated by phase behavior effects. The path by which the binodal is crossed during the process largely determines the final particle size distribution. Crossing near the plait point resulted in particles with a unimodal distribution, whereas crossing on either side resulted in a bimodal particle size distribution due to nucleation and growth in monomer-rich and monomer-depleted phases. Nucleation and growth rate calculations give further support to the theory of particle formation in two phases. Similar results were found in liquid systems designed to mimic the phase behavior of the CO_2/methylene chloride/monomer system. Hydrodynamic effects (e.g., jet breakup) appear to have a secondary effect on resulting particle sizes; large changes in Reynolds number in the CO_2/methylene chloride/monomer system, and changing the antisolvent from supercritical CO_2 to fluorinated liquid solvents did not result in dramatic changes in particle size distributions.

Acknowledgment. This work was supported in part by grants from the Packard Foundation and the NIH. J.L.O. thanks the National Science Foundation for a Graduate Research Fellowship.

LA0208272